SOME ASPECTS OF MOLTEN CARBONATE FUEL CELLS

A.D.S. Tantram, A.C.C. Tseung and B. S. Harris

Energy Conversion Limited, Chertsey Road,
Sunbury-on-Thames, England

The ultimate aim of fuel cell development is a system of acceptable capital cost that can operate in an economic manner on low cost fuels. Although much effort has recently been put into investigating the alternative routes, the high temperature cell remains a favoured prospect.

Of the two main classes of high temperature cells (a) solid oxide electrolyte cells and (b) molten carbonate electrolyte cells, the latter has significant advantages in its lower temperature of operation and in the wider available choice of materials.

Work started at Sondes Place Research Institute and continued at Energy Conversion Limited, has investigated a wide range of different concepts of the molten carbonate cell. These may be broadly classified as follows:-

1. Free electrolyte cells.

2. Trapped electrolyte cells.

   2.1 Porous magnesia diaphragms.

   2.2 "Semi-solid" or "paste" electrolyte diaphragms.

   Non-eutectic type.

   Inert filler type.

Various combinations and compromises between these types are also possible.

In this paper we are concerned in particular with our experiences with cells based on the inert filler type of semi-solid electrolyte diaphragm.

Before discussing this work, it is worth summarising very briefly our main findings with the other types.

FREE ELECTROLYTE CELLS

The three-phase interface is established by the use of dual porosity electrodes run with a pressure differential. We had great difficulty in fabricating electrodes of sufficient strength at the operating temperature to withstand the necessary differential pressure. The factors contributing to this were:- the very high surface tension of the carbonate melt (see Table 1), the desirability of a small coarse pore size to obtain a high reaction area and, particularly with the cathode, limited choice of materials. From preliminary experiments with cell designs suitable for battery construction, it

was also clear that the problem of sealing the carbonate melt would be extremely severe.

Table 1. Surface Tension of Carbonate Melts, Dynes/cm.

°C	Li, Na, K 9, 6, 5 mol ratio	Li, Na 1 1
430	219.8	
480	217	
530	214	233
580	211	230.4
630	208.2	228

MAGNESIA DIAPHRAGM CELLS

In the absence of any commercial source, we developed our own porous magnesia diaphragms.

The main problem that we found with these cells was loss of electrolyte due to creep. It became clear that a much smaller pore size was desirable, coupled with very accurate control of the maximum pore size. This would prove very expensive in practice. An additional economic factor was the necessity for a machining operation on the sintered diaphragms. Sealing problems were also difficult.

SEMI-SOLID ELECTROLYTE. NON-EUTECTIC TYPE

This type[1] depends on choosing a carbonate composition that is well away from the eutectic, so that there is a range of temperature where the electrolyte body is semi-solid. An example is Li_2CO_3 78%, Na_2CO_3 12%, MgO 10%. The function of the small amount of magnesia in this context is to act as a nucleating agent to ensure the formation of small interlocking crystals when the electrolyte body solidifies after casting. The example given has a usable range from about 530°C (conductivity limit) to about 630°C (strength limit). It collapses under its own weight at 670°C and is completely molten at 690°C. Above this temperature, it can be cast into any desired shape and this facility is the main advantage of this type. We have successfully used this electrolyte in the form of discs, spun cast tubes and in a cell design involving the casting of the electrolyte around performed porous electrodes. The disadvantages are the narrow working temperature range and the fact that the solid:liquid ratio changes with temperature, making interface control difficult and uncertain.

SEMI-SOLID ELECTROLYTE. INERT FILLER TYPE

In the normal version an extremely intimate mixture of a carbonate eutectic and a substantial percentage of very finely divided inert filler (e.g. MgO) is densified to form an impervious electrolyte diaphragm.

General Properties

The physical properties are dependent, in particular, on the particle size of the inert filler and on the percentage used.

At the operating temperature, the carbonate component is molten and in this state the material is somewhat analagous to a clay-water system over a particular range of composition.

Under compression the material behaves in typical fashion, there being an initial elastic period (with some hysteresis) leading to a final yield point, which is quite high enough to make the material of practical use (e.g. >50 p.s.i. for 63% MgO). Compressive creep is extremely small, being undetectable in normal use. Figure 1 shows the integrity of a diaphragm after a 20-day cell test at 650°C, in which a sealing pressure of 10 p.s.i. was used.

Shear strength is, however, very low and shear stresses must be avoided in any cell or battery construction with this material.

Optimum composition is dependent in part on the filler particle size and represents a compromise between strength which increases with filler content and conductivity which decreases with filler content, e.g. for 50 w% MgO the diaphragm factor is 2.5 and for 63.5 w% MgO it is 4.0.

There are also rather less definable requirements associated with the setting-up of an optimum three-phase interface at the electrodes. Electrolyte retention is only a problem at the lower end of the range of usable filler content.

The forces holding these diaphragms together are almost entirely surface tension forces and depend upon there being, in practice, an extremely high meniscus length (molten carbonate - inert filler) at the surfaces of the diaphragm. This is demonstrated by the fact that a sample fully immersed in molten carbonate loses virtually all its compressive strength.

FABRICATION METHODS

Cold Pressing and Liquid Phase Sintering

It is not possible to produce high density diaphragms by this method, although rather better results are obtained if the sintering is carried out in vacuum. (See Figure 2).

Three steps normally take place in a liquid phase sintering. (a) Particle rearrangement under the influence of surface tension forces. (b) An increase in density by a solution and reprecipitation process. (c) Solid state sintering of the solid component. In the present case, we are liable to start with a continuous magnesia network which will resist (a). The solubility of magnesia in the molten carbonates is too low for (b) to appreciably occur and the temperature is too low for appreciable sintering of the magnesia (c). These factors explain why high density diaphragms cannot be made by cold pressing and liquid phase sintering.

Hot Pressing

(a) Above the carbonate melting point.

We have had little success with straight moulding of diaphragms by this method, due mainly to extrusion of the material between plunger and mould. Some experiments with injection moulding did, however, indicate that this would be feasible with high precision equipment.

(b) Below the carbonate melting point.

We find that just below the carbonate melting point the material exhibits a high degree of plastic flow and this method enables us to mould diaphragms to a high density without any of the problems of extrusion or sticking to the mould. The great advantage of this method is that it enables us to fabricate a wide variety of shapes to a finish as good as that of the moulding equipment. Figure 3 shows some electrolyte diaphragms made in this way. They are shown "as pressed," some of the graphite used as the mould release agent still being present. They are cavited to form the electrode gas space, baffled to give good gas distribution and have silver current collectors and connecting gaskets pressed on in the same operation. We have also found it possible to form gasporting in the same moulding operation. It is also possible to press on electrodes at the same time, thus giving a complete unit cell from one pressing operation. (Figure 4). We find, however, that the conditions normally used result in an excessive reduction in electrode porosity leading to poor performance. Subsequent attachment of the electrodes is therefore preferred.

Pretreatment of the material is important. The magnesia filler and the alkali metal carbonates are intimately mixed by ball milling and prefired at 700°C to 750°C. This prefiring treatment is to ensure intimate mixing, complete reaction of impurities and complete elimination of adsorbed water, (more about this later). It is important that the prefiring temperature be above the maximum ultimate cell operating temperature. This pretreatment is repeated at least once more. The material is then ground to below 20 mesh to provide the feed for the hot pressing operation. Alternatively, it may be further ground, cold pressed and sintered, to form a "biscuit" blank for the hot moulding operation.

The effects of some of the variables are shown in figure 2.

One of our standard compositions is 63.5% MgO, which was based on measuring the porosity of pure MgO hot pressed under the same conditions and computing the amount of molten carbonate necessary to just fill this porosity. We see that in practice (figure 2) much higher MgO contents can, in fact, be used due to the lubricating action of the carbonate component.

Our normal selected pressing conditions are 5 t.s.i. at 490°C when using binary eutectic (Na and Li carbonates) and at 385°C when using ternary eutectic (Na, Li, K carbonates).

Our density figures for the carbonate melts are:-(t in°C)

For Li, Na

1, 1 mol ratio, $2.030 - 4.30 \times 10^{-4}(t-500)$ g/cc

For Li, Na, K

9, 6, 5 mol ratio, $2.085 - 4.87 \times 10^{-4}(t-400)$ g/cc

Infiltration

An infiltration method has also been used successfully for the fabrication of electrolyte diaphragms. A cold pressed diaphragm of 100% magnesia will break up on infiltration, but the process may be successfully carried out if the starting material contains an appreciable percentage of the alkali metal carbonates. An example is as follows:-

A mixture of magnesia 63.5w% with sodium-lithium carbonates prefired, ground and cold pressed at 10 t.s.i. This diaphragm is sintered at 600°C, cooled and placed on a prepressed disc of 100% sodium-lithium carbonate. The whole is then reheated to 600°C for half an hour. The additional carbonate infiltrates into the diaphragm as it melts. There is some danger that the infiltrating liquid will bypass some of the pores and leave these unfilled, but this can be overcome if the operation is carried out under reduced pressure, a carbon dioxide atmosphere being advisable. Excess electrolyte is ground off the diaphragm after cooling. The product contains 46 w% of the carbonate electrolyte, has a density of greater than 97% of the theoretical and the linear shrinkage is less than 0.5%.

Operating Experience

We will limit ourselves here to points that are specifically relevant to the use of semi-solid electrolyte. We have made and tested some 120 2-1/2" diameter cells (20 cm^2 active area) and about 60 of 4-1/2" diameter (80 cm^2 active area). We have also made some experimental stacks of 4-1/2" diameter, giving about 50 watts output. Figure 5 shows one of these stacks complete with heater and insulation.

A variety of electrode materials have been used, but a typical example would be – for the anode, "B" nickel, granulated, presintered and graded to -100 + 120 mesh – for the cathode, cosintered $Ag/Cu_2O/ZnO$ (25/2.5/72.5% by wt.) and graded –100 + 120 mesh. In both cases these materials are made into a slurry with a silver suspension containing a temporary binder (giving 1% added silver) and applied to the faces of the electrolyte diaphragm in this form. The electrodes are then sintered in situ as the cell is brought up to operating temperature. Typical electrode thickness is 1 mm, porosity 50% on a 3 mm thick electrolyte diaphragm.

As the electrolyte component of the diaphragm melts, it expands to partially wet the electrode and a stable three-phase interface is set up. This process takes rather longer to equilibrate than one might imagine and is illustrated in figure 6, where the internal resistance of a new cell is followed over an initial temperature cycle of 2 hours duration. The extent and location of the three-phase interface will depend on the balance between the surface tension forces in diaphragm and electrodes. It will be affected in particular by the very fine microstructure in the electrode, for instance by the activation treatment mentioned later. These factors are difficult to control and this is one of the disadvantages of this type of cell construction.

Performance and Endurance

We must first of all distinguish between "unactivated" electrodes and those specially activated. The nickel anode may be activated in situ by a controlled partial oxidation, using a small percentage of oxygen in nitrogen such that about 5w% of the nickel is oxidised, followed by reduction with the fuel gas. The effect of such an activation is shown in figure 7.

An electrode activated in this fashion does, however, show a fall in activity with time and after about 60 hours the performance is the same as an unactivated electrode, which would remain unchanged over this period. We have experimented, with some success, with methods of stabilising this activation, but the long term results reported here refer to the lower level of performance. Figure 8 shows the performance obtained with an activated nickel electrode on pre-reacted methane-steam and on hydrogen. Figure 9 shows the effect of the fall in anode activity and the longer term performance deterioration discussed below.

Initial endurance tests with these cells showed that there was a progressive deterioration in performance occurring in the hundreds of hours region. The behaviour was not particularly reproducible and did not show any trend with temperature of operation or with current density and, in fact, similar results were obtained with cells left on open circuit for the bulk of the time. It was suspected that the fall-off was due to deterioration of the electrolyte diaphragms. Physical examination of the diaphragms after the tests, showed the presence of laminar faults. Examples of these are shown in figure 10. It should be noted that we have chosen particularly extreme examples to illustrate the phenomenon, the faults being usually considerably less marked. These faults result in (a) an increased internal resistance and (b) increasing inter-electrode leaks leading to falling performance. Using gas chromatographic techniques we were able to obtain a correlation between falling performance and increasing leaks. The procedure was as follows:-

With the cell on open circuit, hydrogen feed to the anode and air/carbon dioxide to the cathode, the nitrogen content of the anode effluent was analysed. This nitrogen could come by inter-electrode diffusion or by diffusion through a gasket leak from the external air. The cathode feed was then temporarily replaced by methane and the nitrogen estimation in the anode effluent was repeated. In this manner a semi-quantitative measure of both gasket and inter-electrode "leaks" could be obtained. The gasket leak did not normally alter with time and we were, in fact, able to eliminate this, by making the seal directly between the electrolyte diaphragm and the separator i.e. in effect by abolishing gaskets. Figure 11

shows an example of the correlation between falling performance and increasing inter-electrode leak.

Diaphragm deterioration was overcome by ensuring complete elimination of chemisorbed water from the material used for hot pressing. Any still present would be evolved during operation of the cell and initiate the lamination faults. These would tend to get worse with time, due probably to erosion effects arising from chemical combustion of the fuel and oxygen diffusing into the diaphragm. Water is very tenaciously held by magnesium oxide and much longer prefiring times are necessary than might be thought. In addition, the prefired material will quite readily readsorb water and strict precautions have to be taken to ensure that this does not occur. Figure 12 illustrates the stable performance that can be obtained when strict attention has been paid to these factors. The increase in performance seen in the middle of this particular test was not explained. Finally figure 13 shows the absence of faults in an improved diaphragm after a cell test of 450 hours.

Conclusions

Practical cells, based on "semi-solid" electrolyte diaphragms, can be made with promising performance and endurance characteristics. Further improvements are desirable and there are indications that these can be achieved.

Careful battery design should be able to obviate the disadvantages of this type of cell and to exploit its advantages.

The hot pressing fabrication technique should be amenable to mass production methods, since the required conditions are not too far removed from existing plastic moulding practice. This could prove an important factor in achieving low capital cost.

THE ANODE MECHANISM

For the high temperature cell to fulfill its promise considerably higher power densities are required. To be able to take logical steps in this direction a better understanding of the electrode processes and their rate controlling steps is desirable. We are, therefore, taking a fresh look at this problem and the preliminary results are reported here. The anode process was chosen for the initial study, since in practical cells the greater part of the polarisation is normally at this electrode.

Experimental

The test cell used is shown schematically in figure 14. Also included, but not shown, were a reference electrode and a thermocouple pocket. Both the counter electrode and reference electrode were of platinum gauze partially immersed in the electrolyte and both were supplied independently with a 2.5:1 air - carbon dioxide mixture. The electrolyte was an equimolar mixture of sodium and lithium carbonates.

The positioning device enabled the electrolyte crucible to be raised or lowered thus, controlling the degree of electrode immersion. Starting with the electrolyte level below the bottom of the test electrode, the crucible is raised slowly until "first

touch" is registered by an electrical continuity test. The results quoted here are all with a further immersion of 0.1 inches. In addition to this there will be a meniscus about 0.25 inches high.

Initially both nickel and silver-palladium foils were chosen for examination, one point being that the large difference in possible hydrogen diffusion rates through the bulk metal could lead to instructive results. The foil electrodes were 0.005" thick and 1.15 cms wide. The silver-palladium used was the 23% silver alloy. The foils were used as received, with no pretreatment.

The anode compartment was swept with a large excess of hydrogen at 1 atm.

Results and discussion

Figure 15 shows the corrosion curve for the silver-palladium obtained under "white spot" nitrogen, and indicates that only relatively low corrosion currents are possible in the potential range of interest.

Figure 16 compares the current voltage curves for hydrogen oxidation on nickel and silver-palladium at 550°C. The nickel curve was not very reproducible. The reproducibility of the silver-palladium curves is discussed later.

Figure 17 shows plots of E versus log i for hydrogen oxidation on silver-palladium at 550°C and 600°C respectively. It is seen that there is a very well defined linear portion extending over nearly two decades.

At this stage it was noticed that the relationship between E and i was very similar to that between E and x, where x describes the composition of a partially reacted fuel in the manner shown below.

Assume that we start with 1 mol of H_2 and that x mols react with CO_3^{2-},

$$H_2 + CO_3^{2-} = H_2O + CO_2 + 2e$$

and that b mols of H_2 react further with the CO_2,

$$H_2 + CO_2 = H_2O + CO$$

equilibrium being reached.

For 1 atm total pressure, the partial pressures in the resulting mixture are therefore,

$$P_{H_2} = \frac{1 - (x + b)}{1 + x}, \quad P_{H_2O} = \frac{x + b}{1 + x} \quad P_{CO_2} = \frac{x - b}{1 + x}, \quad P_{CO} = \frac{b}{1 + x}$$

and we can write for the water gas equilibrium

$$\frac{(x + b)\, b}{[1 - (x + b)][x - b]} = K \qquad \ldots\ldots\ldots\ldots\ldots\ldots\ldots\ldots (1)$$

At a given temperature this equation can be solved to obtain values of b to correspond with selected values of x. The corresponding partial pressures may then de derived and, from them, the c.rresponding values for E using the equation

$$E = \frac{RT}{4F} \log_e K_o P_{O_2}^* P_{CO_2}^* + \frac{RT}{2F} \log_e \frac{P_{H_2}}{P_{H_2O} P_{CO_2}} \quad \ldots\ldots\ldots\ldots(2)$$

$P_{O_2}^*$ and $P_{CO_2}^*$ refer to the partial pressures at the cathode. K_o is the equilibrium constant for $2H_2 + O_2 = 2H_2O$.

At a given temperature and for constant cathode conditions we can write

$$E = \text{Constant} + \frac{RT}{2F} \log_e \frac{[1-(x+b)]\,(1+x)}{(x+b)(x-b)} \quad \ldots\ldots\ldots\ldots(3)$$

It is found that the plot of E versus $\log_{10}x$ is linear over a wide range and it is the slope (S_x) of this plot that corresponded closely with the observed slopes (S_i) of the initial experimental $E - \log_{10}i$ plots at 550°C and 600°C. These figures are tabulated in table 2.

Table 2. Values of K, S_x, S_i, and α_x.

°C	K	S_x mV	S_i mV	α_x
550	0.219	197	197	0.414
600	0.295	226	233	0.383
650	0.385	246		0.372
700	0.49	262		0.368
887	1	336		0.343

α_x is the value derived from writing $S_x = \frac{2.3\ RT}{2F\alpha_x}$

These considerations suggested the following picture. In the low current region (i.e. down to about 0.95v) the most important factor is the diffusion rate of reaction products away from the reaction site, on the immersed portion of the electrode, through the meniscus to the bulk gas. This rate should be proportional to the concentration difference and so the concentration of products at the reaction site has to build up appreciably before a reasonable diffusion rate is possible. This build up will affect the electrode potential in a similar manner to that defined by equation 3. As the current is further increased the rate of hydrogen diffusion to the reaction site would become the most important factor. Confirmatory evidence for this view is that silver-palladium, which has an additional route for hydrogen diffusion through the bulk metal, supports much higher currents than nickel.

A more precise statement of the hypothesis is as follows:- At a given current the observed polarisation is due to the change in surface concentrations necessary to produce the diffusion rates of both reactants and products to meet the requirements of the processes occurring.

Making the following assumptions:-

The partial pressures of CO_2, H_2O and CO in the bulk gas (H_2 at 1 atm.) are all zero.

The surface concentrations at the reaction site can be described in terms of partial pressures, P_{H_2} etc., in atm.

The diffusion rates are directly proportional to the partial pressure differences.

Rate of discharge of $CO_3^{2-} = i$ $\quad (CO_3^{2-} + H_2 = CO_2 + H_2O + 2e)$ fast.

Rate of formation of $CO = y$ $\quad (H_2 + CO_2 = CO + H_2O)$ fast,

the rates being expressed in units of current, i.e. coulombs/sec. Then we can write,

Rate of H_2 in $= i + y = k_1 (1 - P_{H_2})$ $\quad$ hence $P_{H_2} = \dfrac{k_1 - (i + y)}{k_1}$

Rate of H_2O out $= i + y = k_2 P_{H_2O}$ $\quad$ hence $P_{H_2O} = \dfrac{i + y}{k_2}$

Rate of CO_2 out $= i - y = k_3 P_{CO_2}$ $\quad$ hence $P_{CO_2} = \dfrac{i - y}{k_3}$

Rate of CO out $= y = k_4 P_{CO}$ $\quad$ hence $P_{CO} = \dfrac{y}{k_4}$

The k's involve the diffusion coefficient, Henry's law constant and the geometry of the diffusion path. The units will be coulombs. sec^{-1} $atm.^{-1}$.

For the water gas equilibrium,

$$\frac{(i + y)\, y}{[k_1 - (i + y)][i - y]} = K. \quad \frac{k_2 \cdot k_4}{k_1 \quad k_3} = K^1 \quad \ldots\ldots(4)$$

For the cell e.m.f. at a given temperature

$$E = \text{Const} + \frac{RT}{2F} \log_e \frac{k_2 \cdot k_3}{k_1} + \frac{RT}{2F} \log_e \frac{k_1 - (i + y)}{(i + y)(i - y)} \quad \ldots\ldots(5)$$

We cannot solve these equations without a knowledge of the k values, but a certain amount of information can be obtained using the analogy with the equations in x and b, (1) and (3), which can be solved. We find (a) that S_i will be very little affected by the value of k_1 provided that k_1 is appreciably greater than i + y i.e., provided we are not near the limiting current condition and (b) that S_i will be appreciably affected by the value of K^1. The extent of this variation can be seen by comparing the variation of α_x with K in table (2). To explain the experimental fit noted earlier, $\frac{k_2\ k_4}{k_1\ k_3}$ would have to be fairly close to 1.

Attempts to obtain confirmatory experimental results, however, met with some difficulty. In all cases a well defined linear range on the E – log i plot was found, the individual curves reproduced well with rising and falling current, and the values of S_i in a given series increased with temperature. On the other hand the values for S_i, obtained in different series, done for example on different days, showed a wide scatter. The following figures show the extremes recorded.

(a) At a given temperature (650°C)

Lowest S_i = 165 mV , (α_i = 0.555)

Highest S_i = 530 mV , (α_i = 0.173)

(b) At any temperature.

Lowest S_i = 147 mV , (α_i = 0.536) at 520°C.

Highest S_i = 800 mV , (α_i = 0.121) at 700°C.

At first sight it was difficult to explain these variations on the diffusion theory, since they implied a very wide variation in the value of $\frac{k_2\ k_4}{k_1\ k_3}$ and it was hard to see how this could occur.

It was, however, noticed that the value of S_i was dependent on the history of the anode compartment conditions in the following manner. If the anode compartment had been left for a long period under pure hydrogen, low values for S_i were obtained. If, however, it had been left under carbon dioxide before the tests with pure hydrogen, high values were obtained for S_i. This observation suggested the following explanation. In the former case some decomposition of the carbonate electrolyte in the anode compartment will occur, leaving it CO_2 depleted and rich in M_2O. This will mean that there is a chemical sink available for the carbon dioxide, produced when taking a current, and would be expected to result in a very high value for k_3 (CO_2) as compared with diffusion through the liquid to the bulk gas. There would also be a tendency for $k_2(H_2O)$ to increase for the same reason, but since the equilibrium

$$2\ MOH + CO_2 = M_2\ CO_3 + H_2O \quad \ldots\ldots\ldots\ldots\ldots\ldots\ldots\ldots (6)$$

is well over on the carbonate side we might expect the effect on k_2 to be considerably less marked. If this is true then we can see that the value of K^1 will be considerably reduced and this will result in an abnormally low value for S_i. One can also postulate that when the anolyte has been under CO_2, but starved of H_2O, similar considerations will dictate a low value for k_3 (CO_2) and a high value for k_2 (H_2O) due to the reverse of reaction (6) above. In this case therefore we would expect a high value for K^1 and hence S_i. Confirmatory evidence is that, in the CO_2 deficient condition, unnaturally low open circuit voltages were observed on hydrogen. This is to be expected if the concentration of oxygen ions in the anolyte is increased[2].

Finally the limiting current region was explored for various hydrogen-carbon dioxide mixtures on silver-palladium and the results are shown in figure 18. With pure hydrogen the limiting current region was very unstable.

Conclusions

It is possible to explain the experimental results in terms of a diffusion control mechanism, but further, more rigorously controlled experiments are necessary to obtain a valid quantitative correlation. We postulate that at a given current density the observed polarization is due to the change in surface concentrations necessary to produce the diffusion rates of both reactants and products to meet the requirements of the processes occurring. It follows that in the lower current density region the diffusion rates of the products are the dominant factors and that in the higher current density region the rate of hydrogen diffusion will become dominant. In the latter case the rate of diffusion of hydrogen through the bulk metal can be of great significance.

An essential part of the treatment is the assumption that the water gas shift occurs at the electrode surface and reaches equilibrium.

Any explanation in terms of activation control seems unlikely in view of the wide variation in α_i that was found.

Partial decomposition of the anolyte could strongly influence the diffusion rates of CO_2 and H_2O.

The investigation will continue with studies on other metals and other fuels.

ACKNOWLEDGEMENTS

The authors wish to thank their colleagues, past and present, who have contributed to this work and the Board of Energy Conversion Limited for permission to publish.

REFERENCES

(1) H. H. Chambers and A. D. S. Tantram, British Patent 806592.

(2) J. Dubois and R. Buret, Bulletin de la Societe Chemique de France, 1963, p.2552.

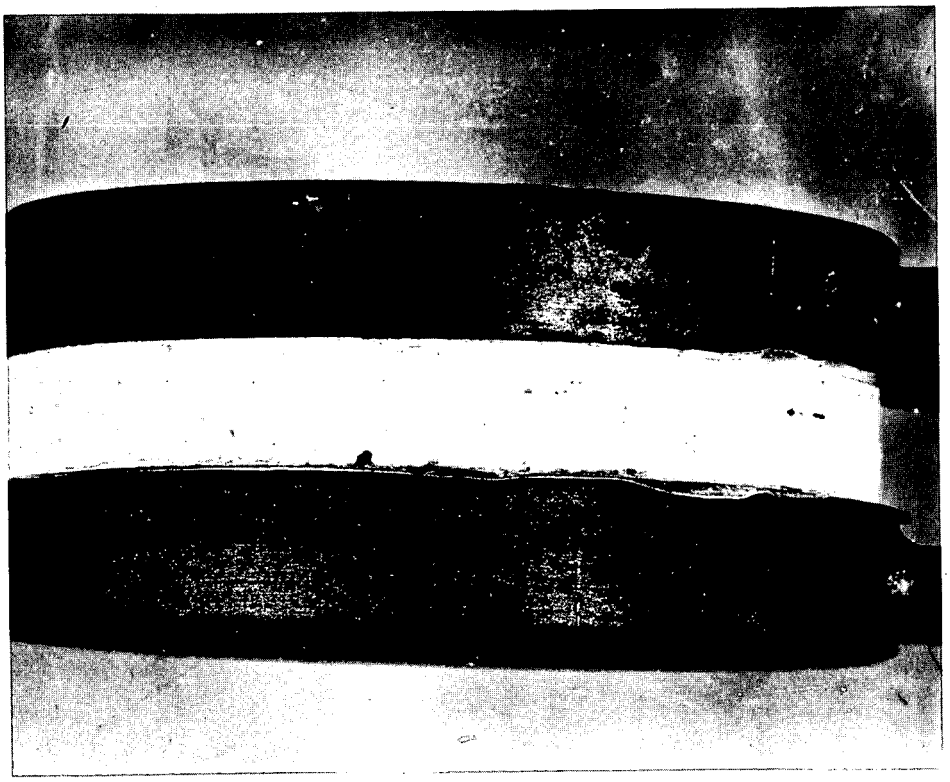

Fig. 1.-CELL AFTER 20 DAYS AT 650°C AND 10 PSI SEALING PRESSURE, SHOWING LACK OF DIAPHRAGM CREEP

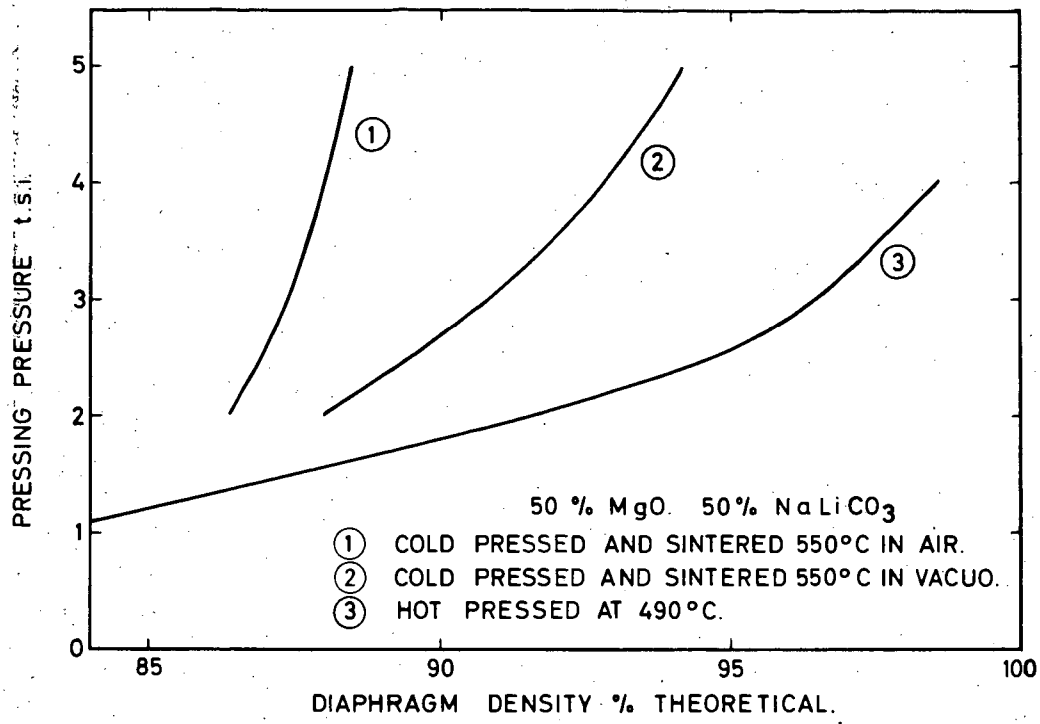

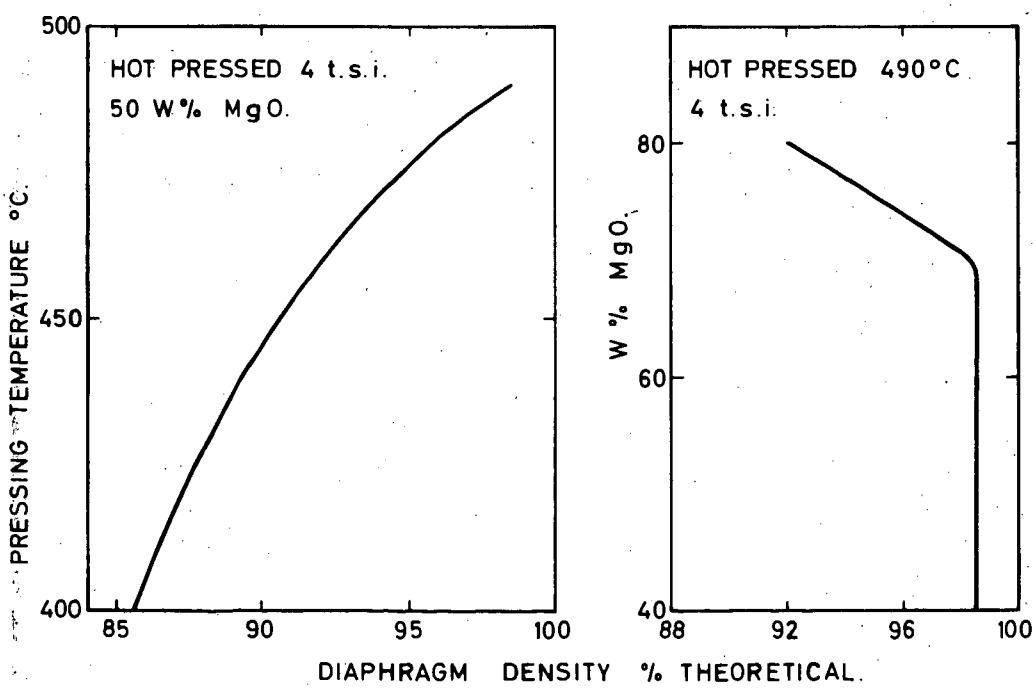

FIG. 2 THE EFFECT OF PRESSING CONDITIONS.

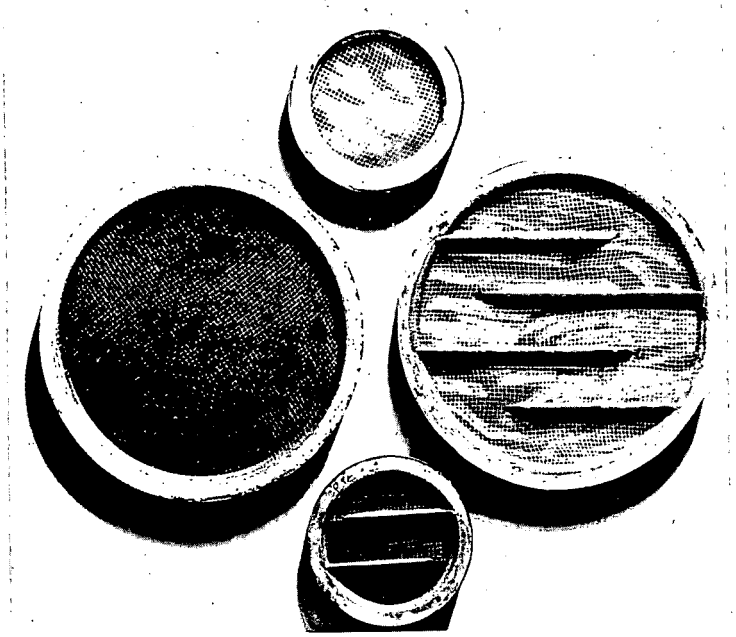

Fig. 3.-HOT-PRESSED ELECTROLYTE DIAPHRAGMS, 2.5" AND 4.6" IN DIAMETER

Fig. 4.-SECTION OF INTEGRAL CELL ELEMENT MADE BY SINGLE HOT-PROCESSING OPERATION

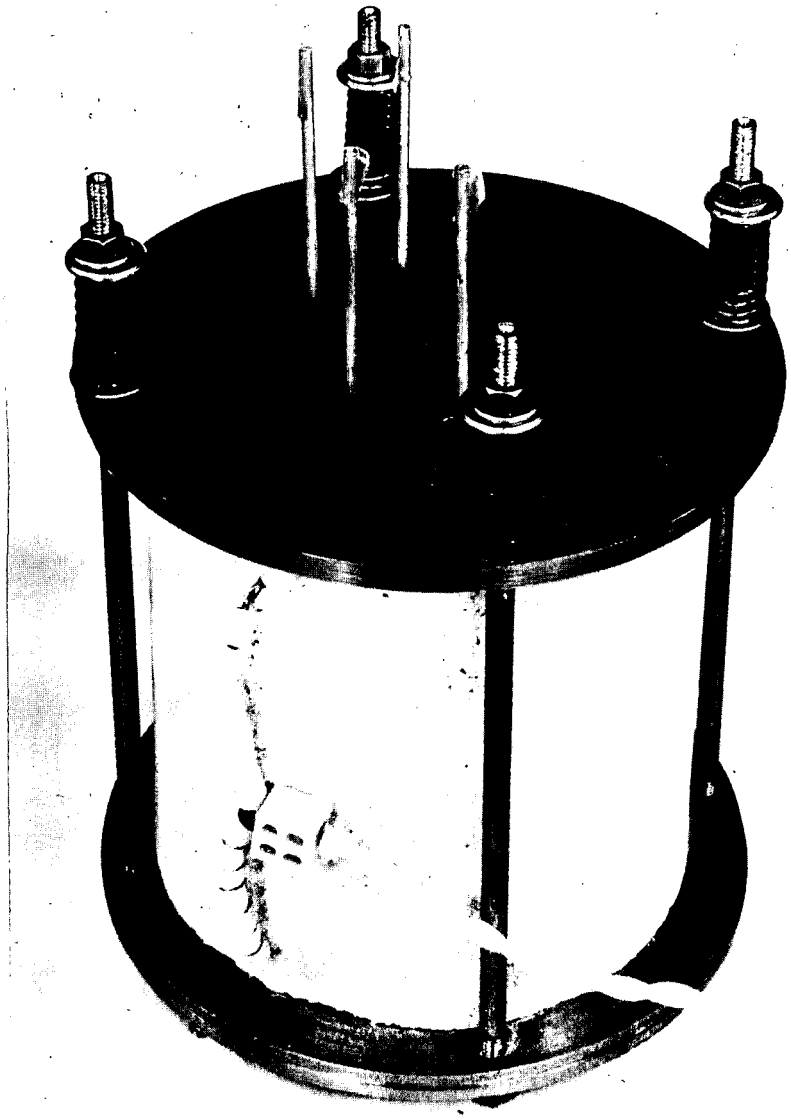

Fig. 5.- FIFTY-WATT BATTERY WITH HEATER AND INSULATION

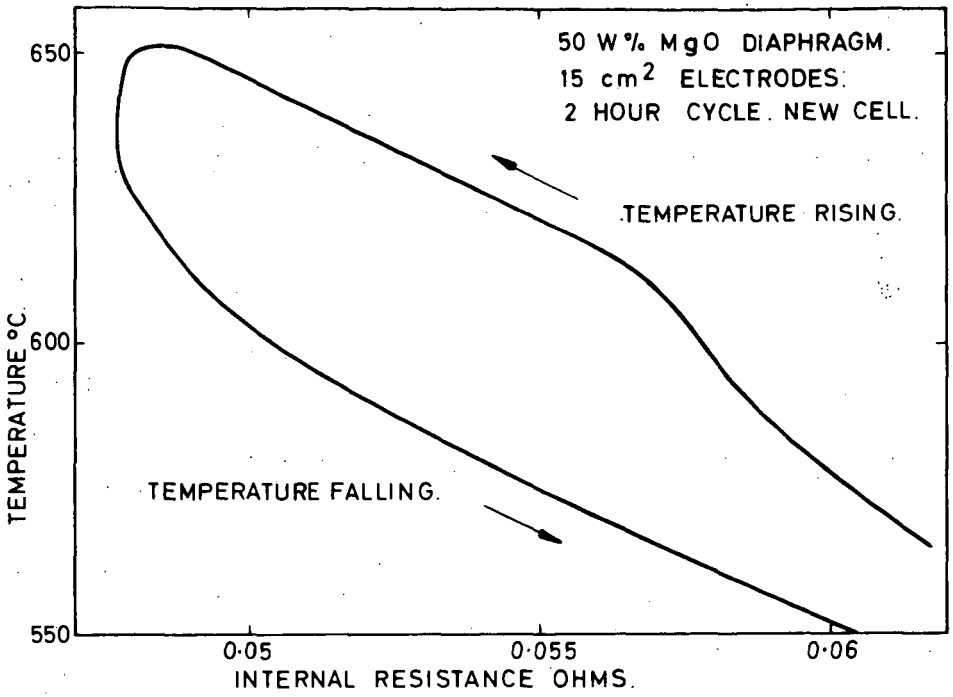

FIG. 6 ESTABLISHMENT OF 3 PHASE INTERFACE.

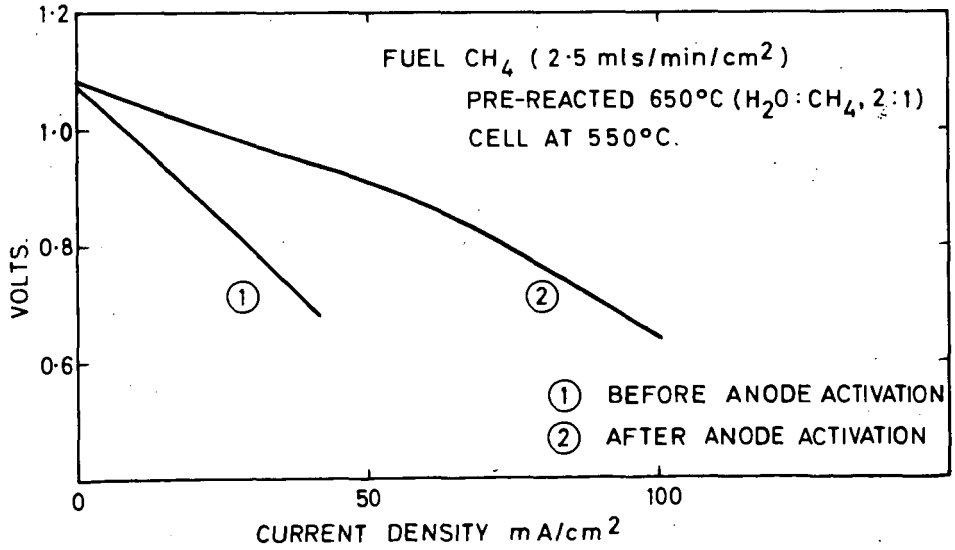

FIG. 7 EFFECT OF ANODE ACTIVATION.

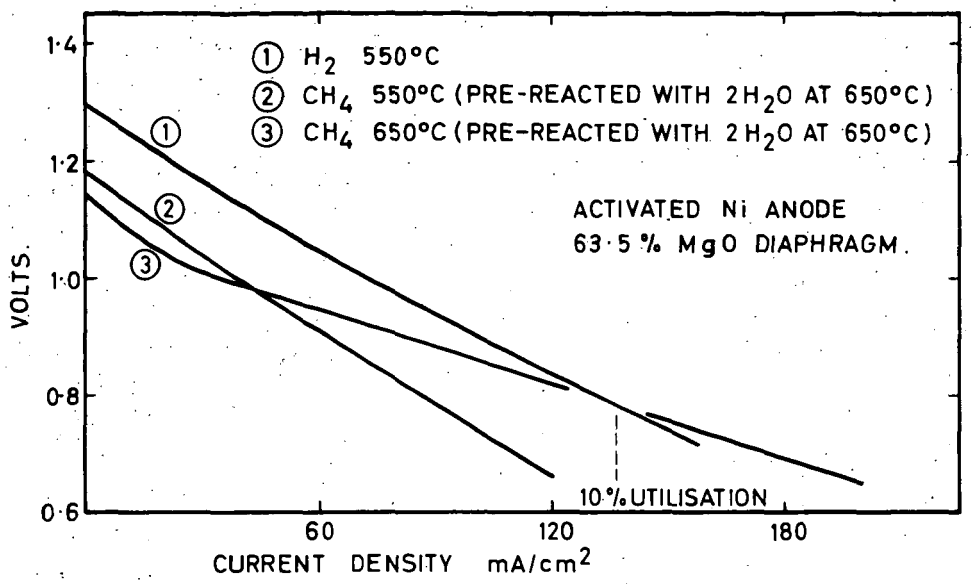

FIG. 8 INITIAL PERFORMANCE CELL H.P. 48.

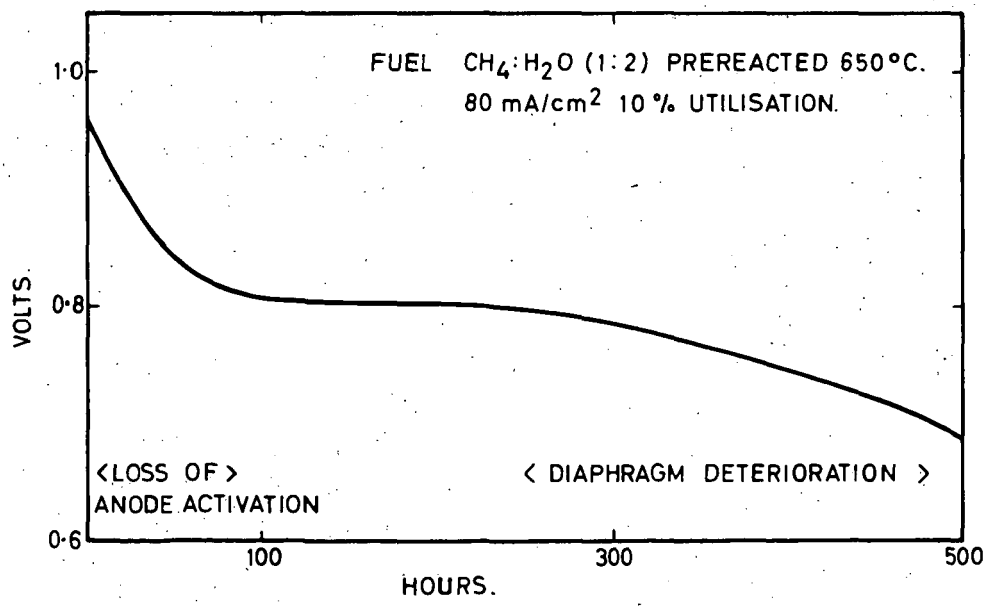

FIG. 9 ENDURANCE OF CELL H.P. 48 AT 650°C.

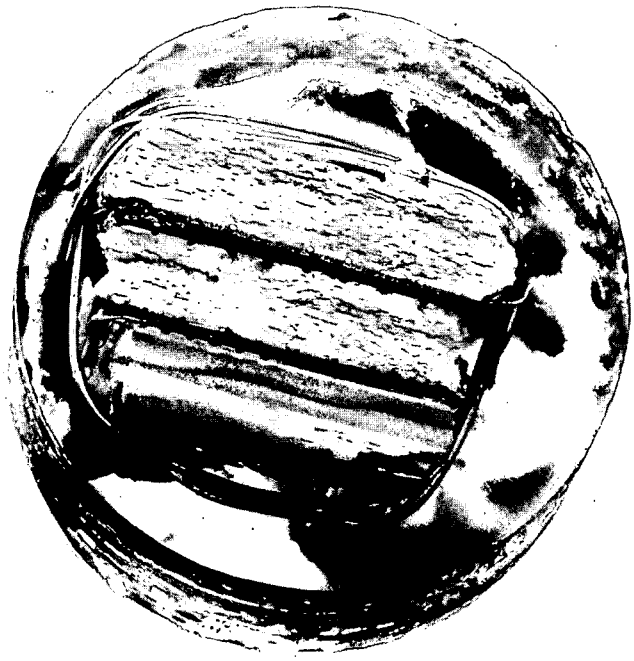

Fig. 10.-SECTIONS OF ELECTROLYTE DIAPHRAGMS AFTER 450 HOURS AT 600°C, SHOWING SEVERE LAMINAR FAULTS

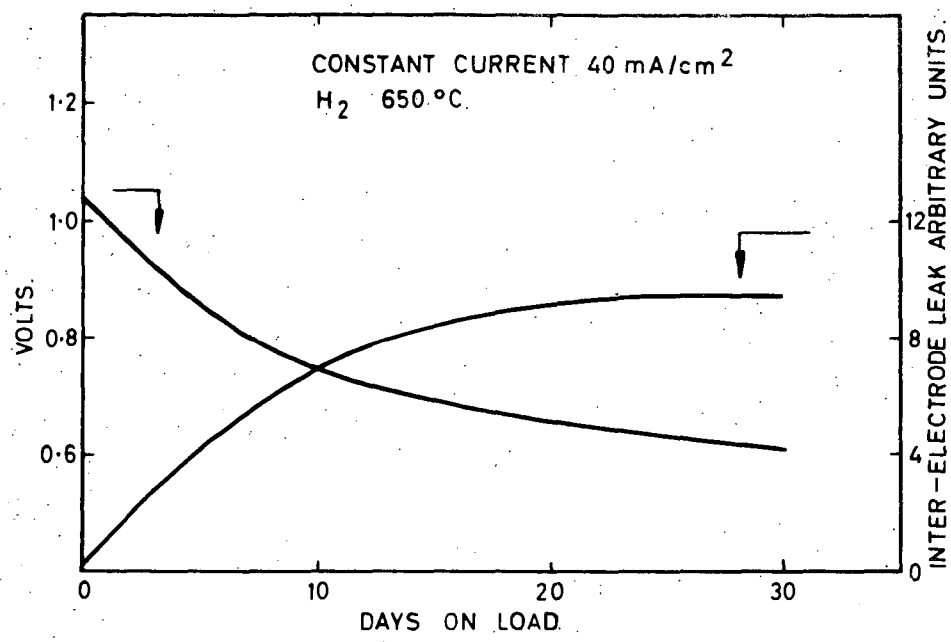

FIG. 11 DETERIORATING DIAPHRAGM. PERFORMANCE—LEAK.

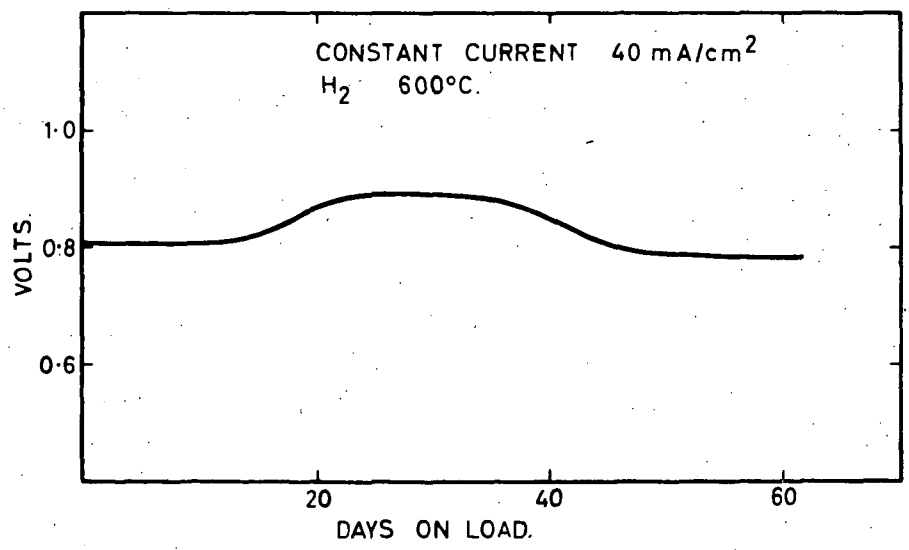

FIG. 12 IMPROVED DIAPHRAGM. ENDURANCE.

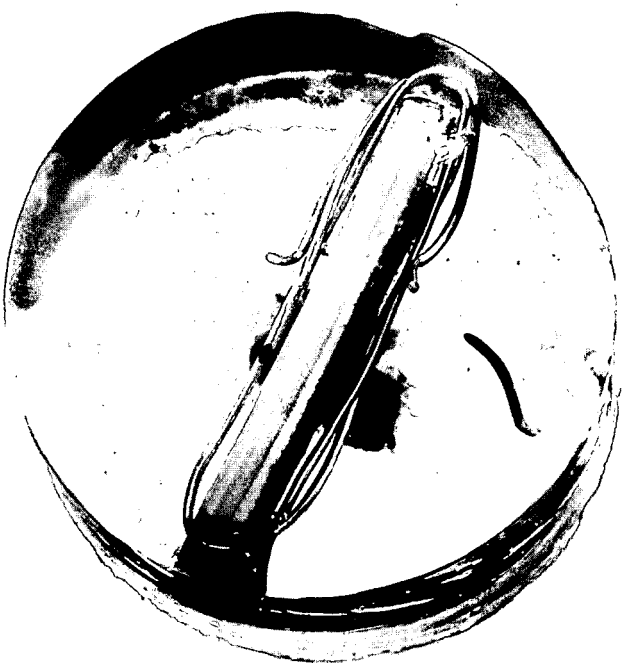

Fig. 13.-SECTION OF IMPROVED DIAPHRAGM AFTER 450 HOURS AT 600°C, SHOWING ABSENCE OF LAMINAR FAULTS (see Fig. 10)

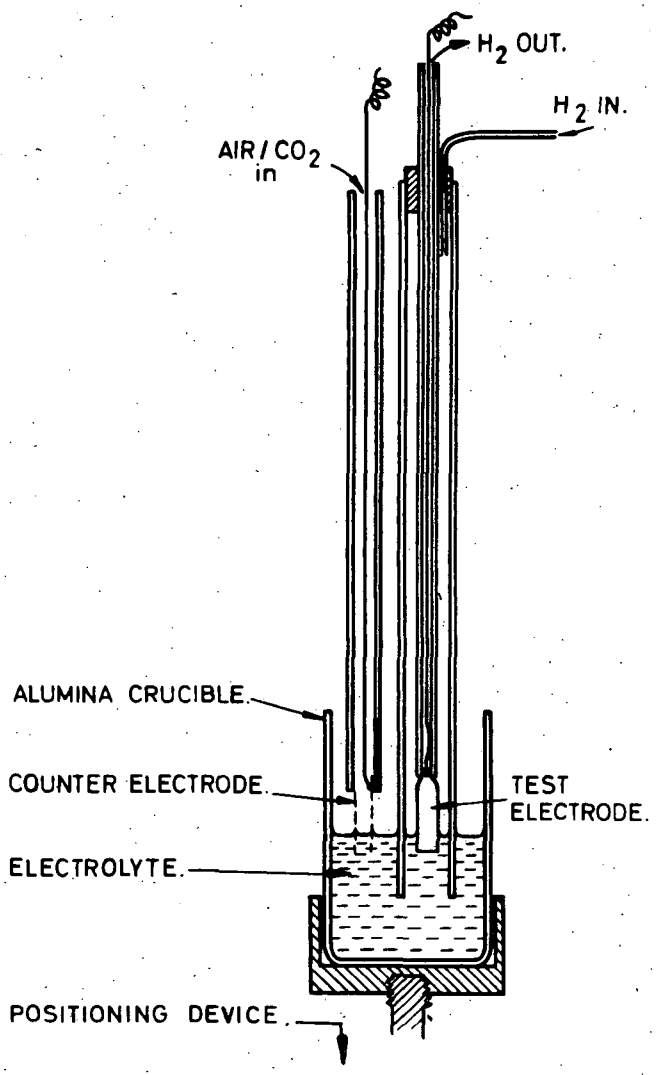

FIG.14 SMOOTH ELECTRODE TEST CELL.

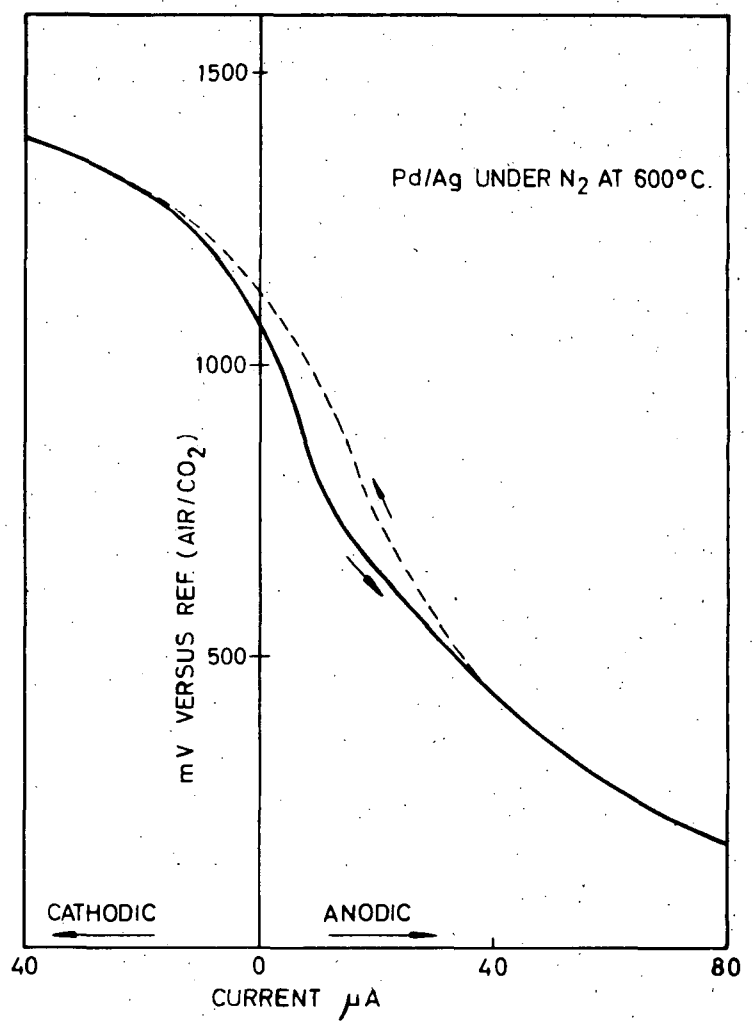

FIG. 15 CORROSION CURVE FOR Pd/Ag.

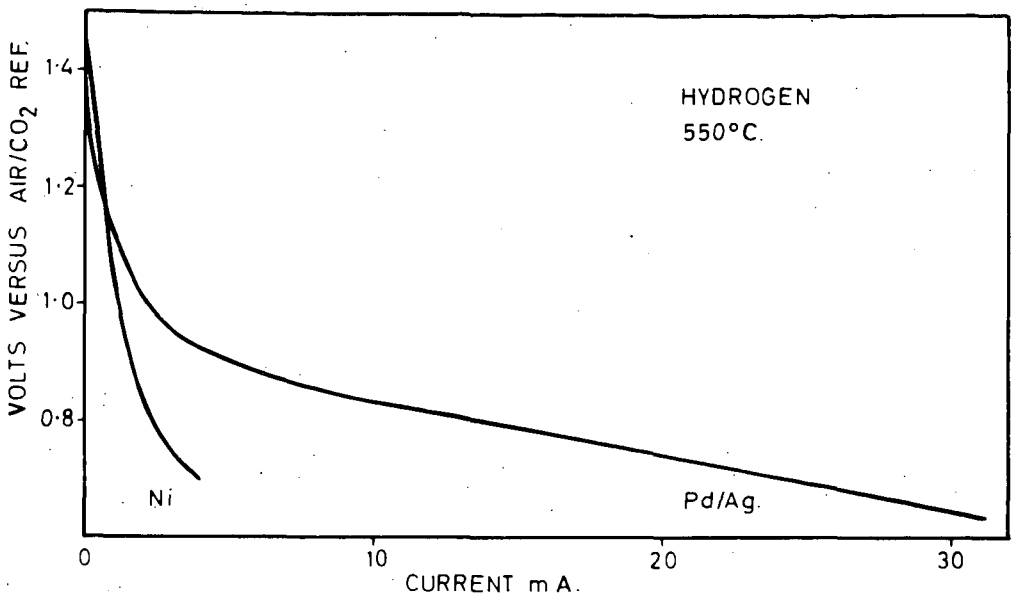

FIG. 16 COMPARISON OF Ni AND Pd/Ag FOIL ANODES.

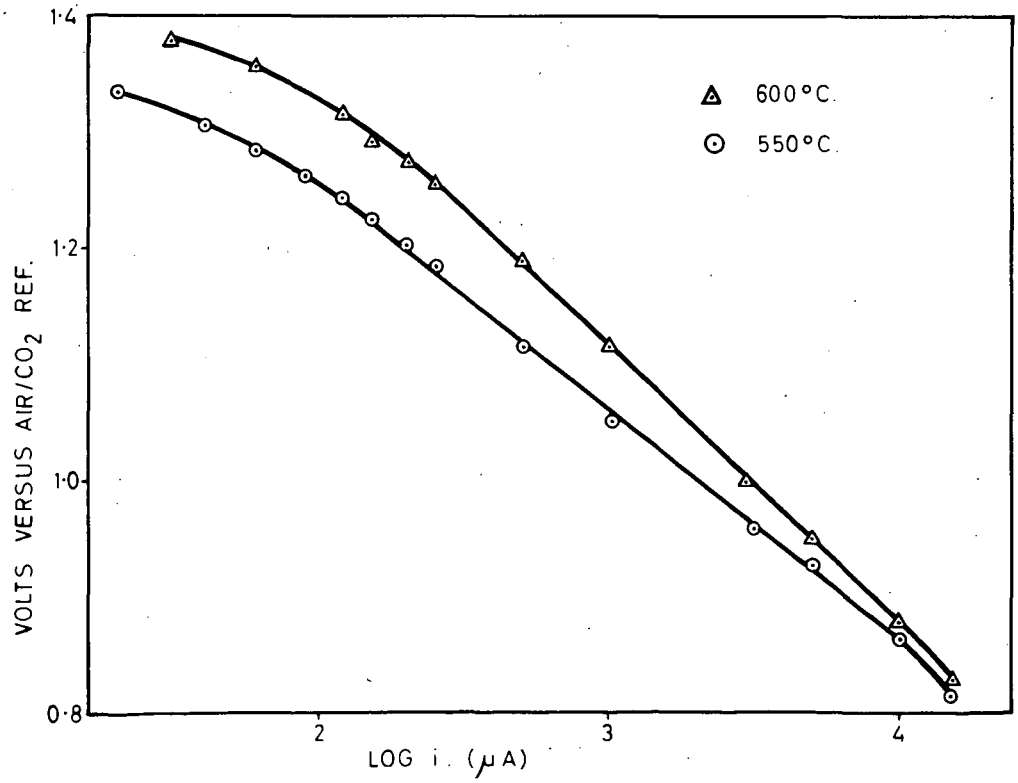

FIG. 17 E – LOG i PLOTS. H_2 ON Pd/Ag.

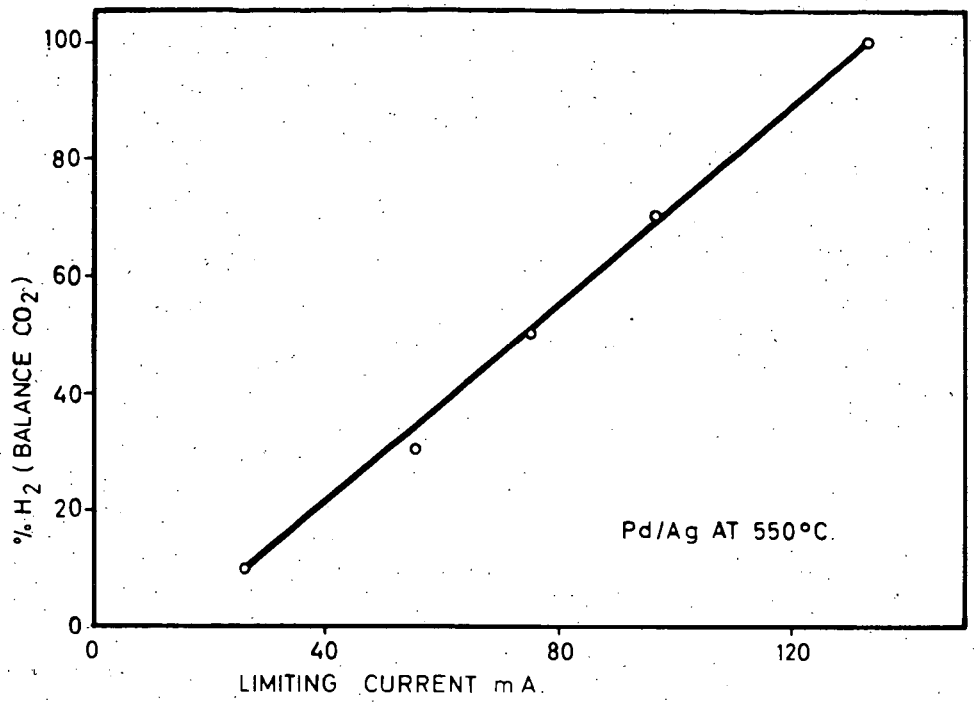

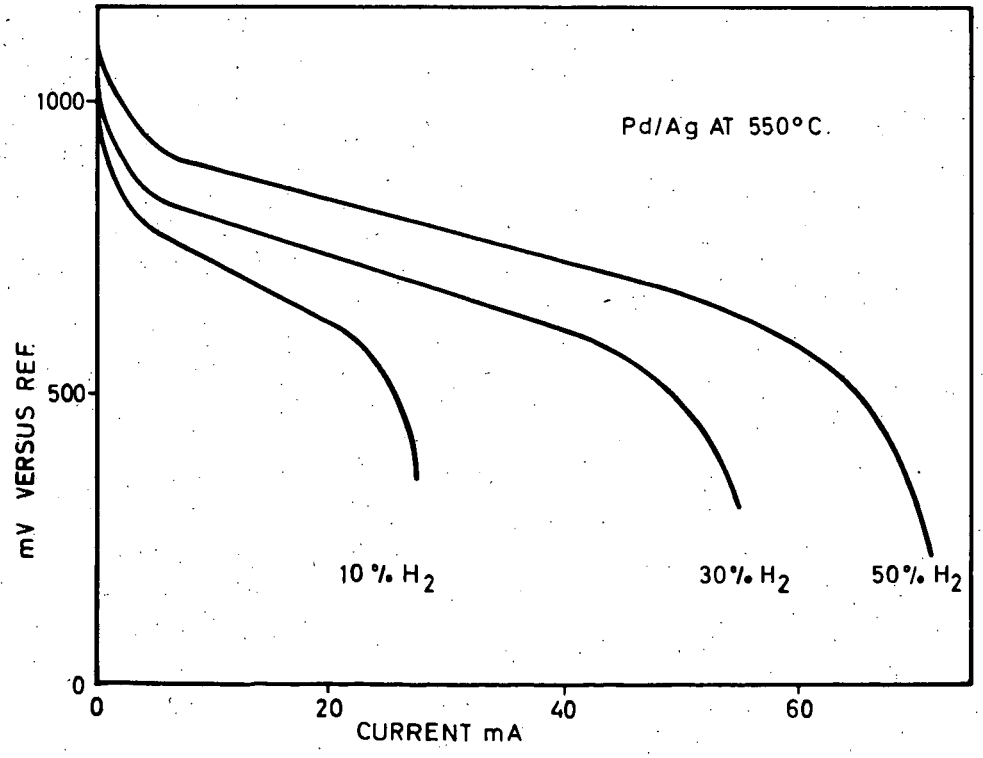

FIG. 18 LIMITING CURRENTS ON Pd/Ag.